From magnetic order to spin-liquid ground states on the $S = \frac{3}{2}$ triangular lattice

J. Tapp,[1] C. R. dela Cruz,[2] M. Bratsch,[3] N. E. Amuneke,[3] L. Postulka,[4] B. Wolf,[4] M. Lang,[4] H. O. Jeschke,[5] R. Valentí,[6] P. Lemmens,[7] and A. Möller[1,*]

[1]*Institute for Inorganic Chemistry and Analytical Chemistry, JGU Mainz, Duesbergweg 10-14, 55128 Mainz, Germany*
[2]*Quantum Condensed Matter Division, Oak Ridge National Laboratory, Oak Ridge, Tennessee 37831, USA*
[3]*Department of Chemistry, University of Houston, Houston, Texas 77204-5003, USA*
[4]*Physikalisches Institut, Goethe-Universität Frankfurt, Max-von-Laue-Straße 1, 60438 Frankfurt am Main, Germany*
[5]*Research Institute for Interdisciplinary Science, Okayama University, 3-1-1 Tsushima-naka, Kita-ku, Okayama 700-8530, Japan*
[6]*Institut für Theoretische Physik, Goethe-Universität Frankfurt, Max-von-Laue-Straße 1, 60438 Frankfurt am Main, Germany*
[7]*Institute for Physics of Condensed Matter, TU Braunschweig, Mendelssohnstrasse 3, 38106 Braunschweig, Germany*

The series of compounds AAg$_2$Cr[VO$_4$]$_2$, with A = Ag, K, or Rb, is layered $S = 3/2$ triangular-lattice (TL) systems in which the magnetic exchange interactions between Cr^{3+} ($3d^3$) ions are mediated by nonmagnetic [VO$_4$]$^{3-}$ entities. Here, the relative orientation of the vanadate is altered with respect to the TL as a function of the A site, which corresponds to an induced symmetry change of the [CrO$_6$] complex. All members of this series of compounds belong to the class of frustrated TL antiferromagnets. We find that the distorted TL (A = Ag) exhibits collinear antiferromagnetic long-range order (LRO) at $T_N \approx 10$ K, whereas the high-symmetry cases (A = K, Rb) evade LRO in zero field down to 0.03 K, the lowest temperature of our experiments. The latter members of the series belong to the undistorted TL and are candidates for spin-liquid ground states presumably not related to Ising anisotropy or dimerization.

I. INTRODUCTION

In recent years, considerable effort has been devoted to the fascinating properties of spin liquids (SLs) [1–4] and their relevance for possible applications such as quantum computation [5]. Some of the most successful approaches towards a rational design of such materials rely on the geometrical frustration of the Heisenberg spin exchange on triangular, kagome, and pyrochlore lattices [2,6–9] or, more recently, on the presence of spin-orbit-induced anisotropic interactions on the honeycomb lattice [10,11]. One important ingredient to novel frustrated materials is the adherence to strict geometrical guidelines, i.e., threefold rotational symmetry for the triangular lattice (TL), which remains a considerable challenge in synthesis. The importance of the symmetry aspect has been pointed out by theory as it effectively suppresses additional terms of the Hamiltonian which may otherwise induce long-range order (LRO) [3,12–14].

The Heisenberg model on the undistorted TL (equilateral triangles of threefold symmetry) with a nearest-neighbor exchange parameter J is a conceptually important model [3,5]. Irrespective of the spin magnitude, LRO is predicted by theory for the antiferromagnetic (AFM) Heisenberg model on the TL with an exceptional ground state that corresponds to a chiral 120° arrangement of magnetic moments [5,14–16]. However, LRO may be suppressed for large single-ion anisotropies on the undistorted Ising AFM-TL in favor of a spin-liquid-like ground state with large remaining entropy [17]. Quasi-two-dimensional materials that present a good realization of the undistorted TL are rare. Examples for Heisenberg systems with very weak single-ion anisotropies are ACrO$_2$ [18], RbFe[MoO$_4$]$_2$ [19], and AAg$_2$Fe[VO$_4$]$_2$ [20]. The latter Fe compounds belong to the class of XY Heisenberg TLs and

order antiferromagnetically around 3 K. For ACrO$_2$ a very small uniaxial anisotropy has been reported, and the ground state represents the solution for the easy-axis Heisenberg model on the TL [21]. Even for the most prominent Ising-ion candidate of the $3d$-ion series, Co^{2+}, chiral 120° LRO has been established (see, for example, Ba$_3$CoSb$_2$O$_9$ [13]).

Beyond the single-ion anisotropy other approaches have been considered to effectively destabilize LRO on the TL. These include (i) spatial anisotropy leading to different nearest-neighbor coupling constants (J_1, J_2) and (ii) further couplings beyond nearest-neighbor two-spin exchange. It has been theoretically shown for $S = 1/2$ systems that SL ground states can be realized for very large differences or certain ratios of J_1 and J_2 [22,23]. As spatial anisotropies are not expected for the undistorted TL, scenario (ii) with multiple-spin exchange could apply [24,25]. Such consecutive exchange processes can effectively suppress AFM LRO as these induce a ferromagnetic component [26,27]. The unambiguous detection is far from trivial as it modifies the physical properties only gradually. Nevertheless, higher-order exchange has been proposed for systems in which effective Coulomb correlations are weaker and/or the exchange path involves several ions [28].

In the present study we focus on members of the AAg$_2M$[VO$_4$]$_2$ series of compounds which exhibit tunable ion sites: A and M [20,29,30]. For the magnetic ion (M site) we have chosen the Heisenberg ion Cr^{3+} ($3d^3$) here because of its extremely small single-ion anisotropy and its orbitally nondegenerate ground state, $^4A_{2g}$, in an octahedral ligand field. The tuning of the magnetic exchange interactions through (M $3d$-O $2p$-V $3d$-O $2p$-M $3d$) hybridization is accomplished by the size of the nonmagnetic ion on the A site. Thereby, rotation and/or tilting of the linker [VO$_4$]$^{3-}$ occurs (see Fig. 1). Here, we present experimental data on a novel insulating Cr series, reporting the suppression of LRO and evidence for a SL-like state due to high-symmetry exchange on the $S = 3/2$ AFM TL.
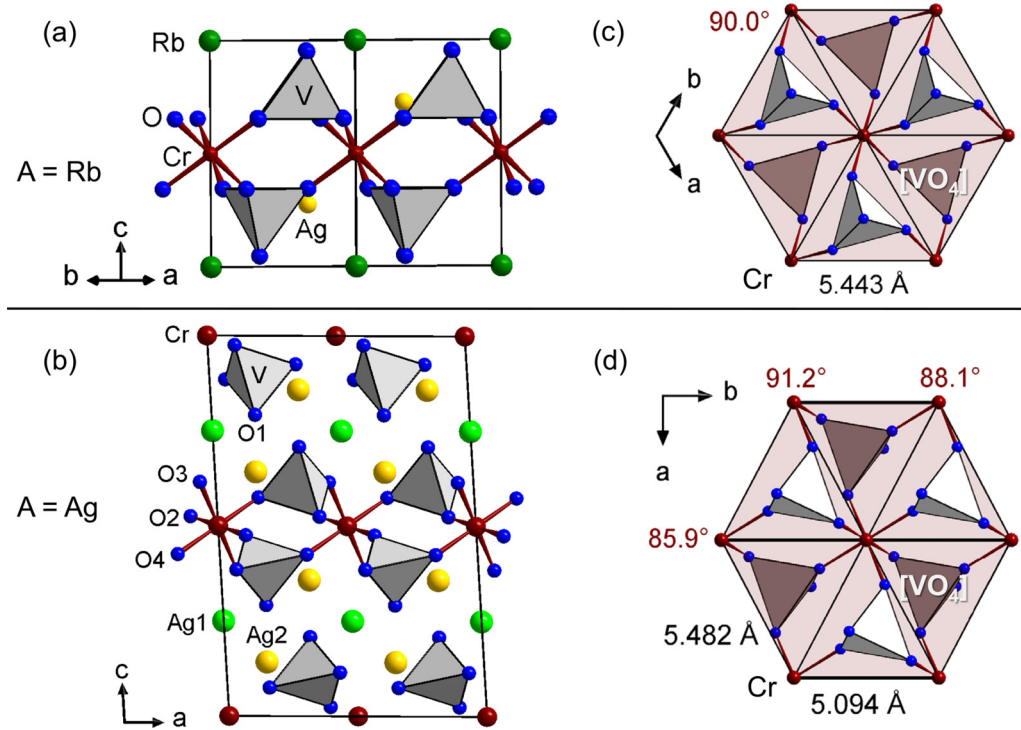
*Corresponding author: angela.moeller@uni-mainz.de

FIG. 1. Left: Crystal structures of (a) RbAg$_2$Cr[VO$_4$]$_2$ ($P\bar{3}$) and (b) AgAg$_2$Cr[VO$_4$]$_2$ ($C2/c$). Right: Cr atoms linked via [VO$_4$] entities on the TL: (c) undistorted case for A = Rb and (d) distorted case for A = Ag. The Cr-Cr distances (black) and O-Cr-O angles (red) are given for comparison.

II. EXPERIMENTAL DETAILS

The samples have been obtained from the initial reaction of K$_2$CO$_3$ (Rb$_2$CO$_3$ or Ag$_2$O) with Cr$_2$O$_3$ and AgVO$_3$ in molar ratios of 1 : 1 : 4 at 753 K, followed by consecutive annealings of pressed pellets at approximately 773 K. The sample quality has been checked by powder x-ray diffraction (Cu K_α radiation, Bruker D 5000 or XPert Pro PANanalytical instruments). The neutron diffraction measurements were done using the HB2a high-resolution powder diffractometer housed at the High Flux Isotope Reactor, Oak Ridge National Laboratory. The pelletized powder samples were measured as a function of temperature using a ^{3}He insert. The collimation used for the measurement was open-open-12$'$ before the monochromator, sample, and detector, respectively, with a Ge[113] wavelength of 2.406 Å. X-ray and neutron data were refined using the program FULLPROF [31].

The dc susceptibility measurements of pressed powder samples were carried out on a physical properties measurement system (PPMS, Quantum Design) using the vibrating sample magnetometer option and a commercial superconducting quantum interference device magnetometer (MPMS). The measurements were performed in the range of 2 K $\leqslant T \leqslant$ 300 K in zero-field-cooled (ZFC) and field-cooled (FC) modes at a field of 0.1 T (see below) and up to 1 T. Field-dependent magnetization data were collected at 2 K in fields up to 8 T. The experimental data were corrected for the contribution of the sample holder, which was determined in an independent experiment and for temperature-independent diamagnetic core contributions [32]. For measurements of the ac susceptibility χ_{ac} down to $T = 0.031$ K and magnetic

fields up to 10 T, an ultrahigh-resolution ac susceptometer, adapted to a ^{3}He-^{4}He top-loading dilution refrigerator, was used. Specific-heat measurements were performed using a PPMS instrument within a temperature range of 2–300 K in magnetic fields of 0–8 T. Phonon contributions were subtracted from the specific-heat data by using the nonmagnetic structural analogues with M = In and A = Ag, K, Rb.

III. RESULTS AND DISCUSSION

A. Crystallographic and magnetic structures

We refined the crystal structures of AAg$_2$Cr[VO$_4$]$_2$, with A = Ag, K, and Rb, from powder neutron (NPD) and x-ray diffraction data. For further details, we refer to the Supplemental Material [33]. The compounds crystallize in the space groups $P\bar{3}$ for A = K, Rb and $C2/c$ for A = Ag (Fig. 1). The prominent feature of these structures is a TL of magnetic Cr^{3+} ions ($S = 3/2$) linked by nonmagnetic vanadate units, [VO$_4$]$^{3-}$, as shown in Figs. 1(c) and 1(d). The two structure types differ in the local symmetry of the [CrO$_6$] units: D_{3d} symmetry with O-Cr-O angles of 90° (Rb) and 89°/91° (K) for $P\bar{3}$ (undistorted TL) versus C_{2v} symmetry with O-Cr-O of 85.9°, 88.1°, 91.2° (Ag) for $C2/c$ (distorted TL). In the former case the connecting vanadate units are coplanar with the TL, whereas in the latter case they are tilted with respect to the axis perpendicular to the TL. Thus, the two structures differ in terms of the ideal equilateral TL ($P\bar{3}$, A = K, Rb) with Cr-Cr distances of 5.443 Å and a distorted TL ($C2/c$, A = Ag) with 5.094 and 2 × 5.482 Å. The interlayer distance along the stacking direction (c axis) is 7.173 Å (Ag), 7.236 Å (K),

and 7.345 Å (Rb), respectively, and follows approximately the increasing ionic size of the A-site cations.

In Figs. 2(a) and 2(b), we show the measured neutron diffraction data at 5 K, 2 K, and 260 mK for the undistorted TL ($P\bar{3}$, RbAg$_2$Cr[VO$_4$]$_2$). The crystal structure contains two independent O atoms. One links the Cr and V atoms within the TL, whereas the other O atom connects exclusively the nonmagnetic cations. Therefore, the magnetic exchange can be assigned to a single J parameter for the nearest neighbors. The retained threefold symmetry down to the lowest measured temperatures makes this compound an exceptional candidate for geometrical frustration scenarios. Thus, one expects significant suppression of LRO in comparison to a distorted TL (see below A = Ag). For A = Rb we observe in the neutron diffraction experiments down to 260 mK only structural reflections [Bragg positions (001), (100), and (101) below $Q = 1.7$ Å^{-1}; Fig. 2(b)]. Neither magnetic short-range order nor LRO down to 260 mK is detected within the experimental resolution [see difference plot in Fig. 2(b)].

In contrast, the distorted TL orders antiferromagnetically around $T_N \approx 10$ K. Figure 2(d) shows unambiguously additional magnetic reflections at 2 K in comparison with the structural reflections observed at 20 K. The propagation vector of the magnetic structure for AgAg$_2$Cr[VO$_4$]$_2$ has been derived as $k = (\frac{1}{2},\frac{1}{2},0)$. The reduced magnetic moment per Cr^{3+} amounts to 2.06μ_B ($z = \frac{1}{2}$) and 2.35μ_B ($z = 0$). We have fitted the order parameter β of the collinear AFM phase by using the expression $y = |T/T_N - 1|^\beta$, where T_N equals the Néel temperature and y are the normalized counts per 200 s for the magnetic reflection ($\frac{1}{2}\frac{1}{2}0$) at $Q = 0.6967$ Å^{-1} [see inset of Fig. 2(d)]. The derived parameter, $\beta = 0.33(1)$, for this fit is close to the Heisenberg solution for the TL, $\beta = 0.35$. It differs from the Ising value of $1/8$ and the mean-field value of 0.5 [15].

In Fig. 3 we show the spin structure with the spins canted out of the TL plane. Note the AFM alignment of the spins along the shortest Cr-Cr distance, which is equivalent to the b-lattice constant. The two directions [110] and [−110] turn out to be aligned differently, despite having the same Cr-Cr distances. Inspection of the O-Cr-O angles reveals the difference between the two crystallographic directions: 91.2° and 88.7° in [110] and [−110], respectively [see also Fig. 1(d)]. Thus, the relative orientation of the vanadate can be considered the crucial ingredient to account for the nonequivalent magnetic exchange interactions. In the Ag compound (distorted TL) four crystallographic distinguishable O atoms exist. Out of these, three (O2, O3, O4) are exclusively connected to chromium. The ordered magnetic moment lies in the plane defined by Cr, O3, and O4 (Fig. 3). In the case that the magnetic exchange is mediated exclusively via O3 and O4 (represented by the [−110] direction), a ferromagnetic (FM) alignment of the ordered magnetic moments is observed. In contrast, the other two Cr-Cr connectivities along [010] and [110] are bridged by the combinations O2-O3 and O2-O4, respectively. For this case, the moments are found to align AFM. The alternating change in orientation of the Cr-O3-O4 plaquette along the c axis is a result of the space-group symmetry ($C2/c$). Accordingly, the ordered magnetic moments are canted with respect to the stacking direction. Furthermore, a FM alignment

of these ordered moments along [001] is established and also supported by *ab initio* calculations below.

B. Magnetic properties

We proceed now with the magnetic properties of the series of compounds AAg$_2$Cr[VO$_4$]$_2$ as shown in Fig. 4. In all cases an effective magnetic moment of $\mu_{\text{eff}} = 3.8\mu_B$ at room temperature is observed, which is consistent with the expectation for a $S = 3/2$ paramagnet. For all systems, the experimental susceptibility down to 2 K [Fig. 4(a)] is systematically smaller than the one calculated on the basis of a ligand field approach [34] for a single-ion complex of D_{3d} symmetry in zero field. Thus, the dominant exchange is AFM throughout the series. We derive Curie-Weiss temperatures of $\Theta_{CW}^{Ag} \approx -32$ K, $\Theta_{CW}^{K} \approx -20$ K, and $\Theta_{CW}^{Rb} \approx -10$ K from fits in the high-temperature range. To determine the magnetic coupling constants, we fitted our data to a high-temperature series expansion (HTSE) [35] based on an $S = 3/2$ TL with Heisenberg interaction and g factors (1.96) derived independently from EPR measurements: $J^{Ag} \approx 3$ K, $J^{K} \approx 1$ K, and $J^{Rb} \approx 0.5$ K, respectively.

These J values for the K and Rb systems determined using the HTSE agree very well with the ones obtained from the corresponding saturation fields $B_s(0)$ (see Supplemental Material). With the relation $B_s(0) = 9SJ$ we derive $J^K = 1.5$ K and $J^{Rb} = 0.6$ K. Note the small values of the exchange coupling constants due to the Cr-Cr interaction path via the [VO$_4$] entities. The relative differences in J are significant considering that the average in-plane Cr-Cr distances of the series are almost identical (see above). More pronounced is the relative orientation of the vanadate which renders the J value, i.e., with a ratio of 6 for J^{Ag}/J^{Rb}. It is also quite remarkable that a significant difference in $\chi(T)$ is observed for the K and Rb compounds ($P\bar{3}$). One may relate the enhancement in χ or suppression in terms of J as an effective addition of a ferromagnetic component, which seems to be more pronounced once the [CrO$_6$] entity is close to ideal O_h symmetry (A = Rb).

In the case of A = Ag a broad maximum in $\chi(T)$ around 20 K followed by a kinklike anomaly at $T_N \approx 10$ K indicates LRO well in line with the neutron and specific-heat data (see below). The AFM exchange on a TL results in competing magnetic interactions, which may be expressed by the ratio $|\Theta_{CW}/T_N| = f$ [9]. For the distorted TL we find $|\Theta_{CW}^{Ag}/T_N^{Ag}| \approx 3$, which corresponds to a moderate frustration.

Figure 4(b) shows the low-temperature ac susceptibility for RbAg$_2$Cr[VO$_4$]$_2$ in emu per mole, similar to Fig. 4(a). In zero field $\chi_{ac}(T)$ exhibits a broad rounded maximum at $T \approx 1$ K and remains constant below $\approx$300 mK. There are no indications for a magnetic phase transition down to the lowest temperature of our experiment of 0.031 K. Upon increasing the magnetic field to 3 T the maximum shifts to lower temperatures, and finally, the ac susceptibility becomes constant below 300 mK. Full polarization [see Figs. 4(b) and 4(c)] is achieved at temperatures below 300 mK in applied fields of 5.5 T with significantly reduced χ_{ac} values. An important experimental finding is the observation of hysteric behavior for temperatures below 0.2 K and fields of 0.5 and 2 T. This is consistent with the opening of a hysteresis in
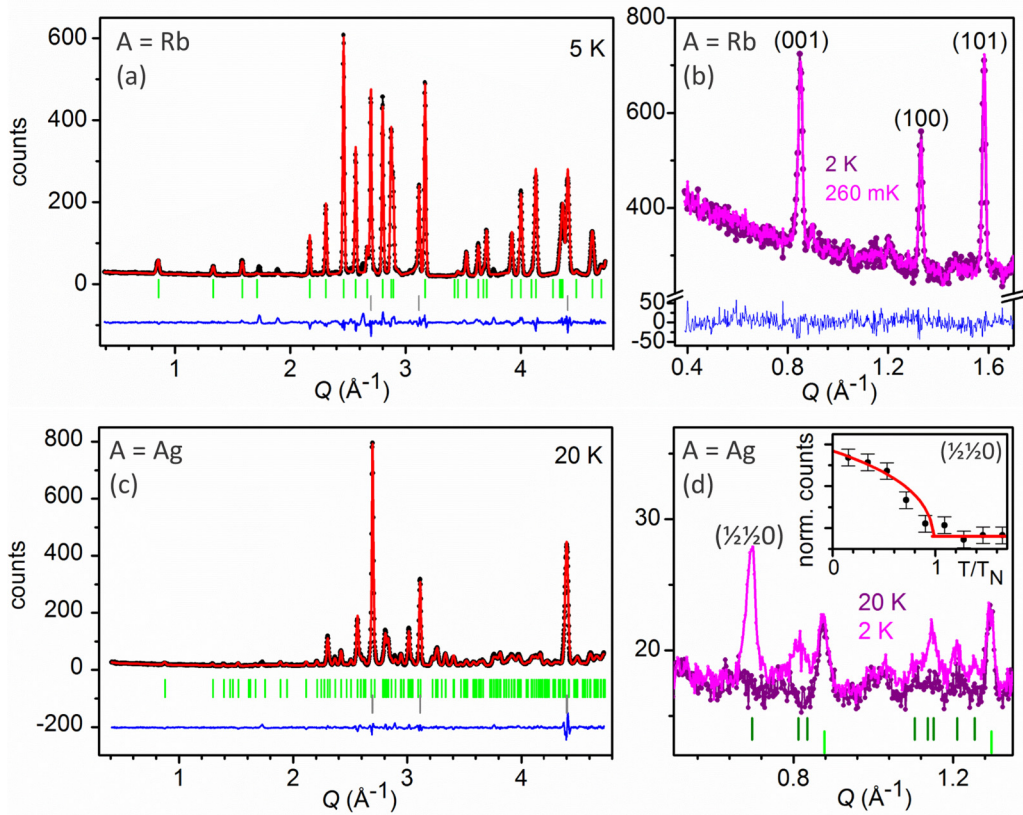
FIG. 2. Rietveld refinement of the crystal structures of (a) RbAg$_2$Cr[VO$_4$]$_2$ ($P\bar{3}$) and (c) AgAg$_2$Cr[VO$_4$]$_2$ (C2/c); black: NPD data, red: simulated pattern, green: structural Bragg positions, gray: Bragg positions for aluminum (container), and blue: difference of observed minus calculated. (b) Comparison of NPD for A = Rb at 260 mK and 2 K, with the difference (blue). (d) Comparison of NPD data for A = Ag at 2 and 20 K, with structural (green) and magnetic (olive) Bragg positions. The inset shows a fit of the order parameter for the magnetic reflection $(\frac{1}{2}\frac{1}{2}0)$; see text.

$\chi_{ac}(B)$ in field-dependent measurements [Fig. 4(d)] in a similar field range. We interpret this behavior as the occurrence of a field-induced ordered magnetic phase in this temperature and

field range for A = Rb. This interpretation is further supported by the ac susceptibility data displayed in Fig. 4(d), which show $\chi_{ac}(B)$ at 0.038 K measured with increasing and decreasing
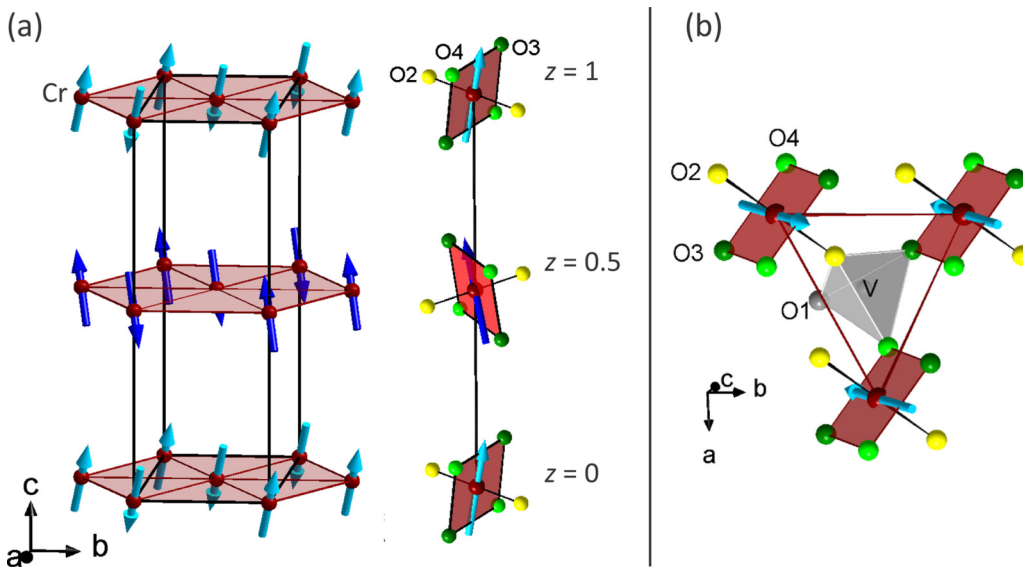

FIG. 3. (a) Magnetic spin structure of the collinear AFM for A = Ag. (b) The ordered magnetic moment given with respect to the relative orientation of the [CrO$_6$] complex along [001] and for one unit of the TL.

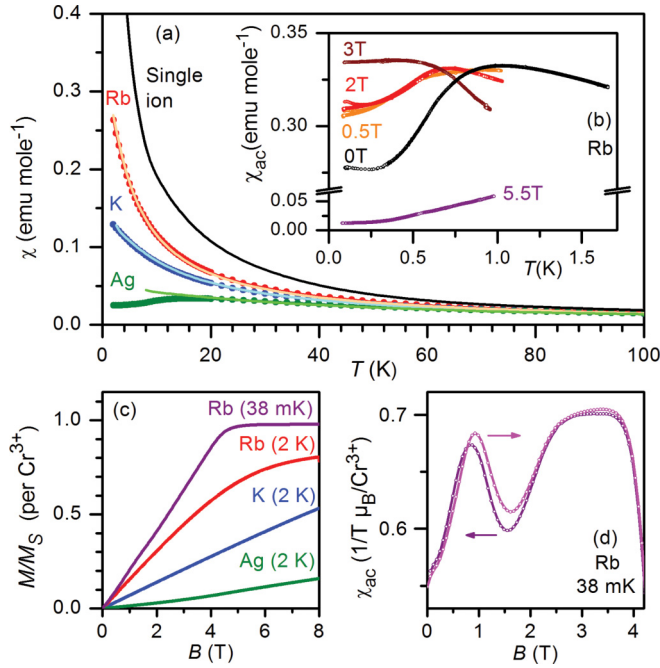FIG. 4. (a) Susceptibility data below 100 K for $A\mathrm{Ag}_2\mathrm{Cr}[\mathrm{VO}_4]_2$, with A = Ag (green), K (blue), Rb (red), measured in a 0.1-T ZFC mode in comparison with the calculated single-ion data and fits to a HTSE for the TL (respective lines to the data). (b) $\chi_{ac}(T)$ for A = Rb below 1.7 K at various applied fields. (c) Magnetic moment divided by the saturated moment per Cr^{3+} vs the applied field for A = Ag, K, Rb. (d) Hysteretic behavior of $\chi_{ac}(B)$ with increasing and decreasing fields (indicated by arrows) for A = Rb at 38 mK.

FIG. 5. Left: Field dependence of the magnetic part of the specific heat divided by the gas constant R for $A\mathrm{Ag}_2\mathrm{Cr}[\mathrm{VO}_4]_2$, with A = Ag (top), K (middle), Rb (bottom). Right: Respective magnetic entropy above 2 K. Note that the individual curves are normalized to reach $S_m^{\max} = R\ln 4$ at $T = 50$ K.

magnetic fields. Both curves exhibit a pronounced maximum around 1 T accompanied by hysteretic behavior in the field range 0.5 T < B < 2.5 T, which slightly shifts to higher fields and becomes more pronounced with increasing temperature (see also Ref. [33]). Such temperature and field dependence of $\chi(T,B)$ is not expected for a 1/3 plateau. This anomaly is absent for higher temperatures, e.g., at 2 K. The magnetization data for the series A = Ag, K, and Rb are given in Fig. 4(c). The individual J values derived above manifest themselves in different initial slopes of the $M(B)$ curves at 2 K as well as differences in the saturation fields. Magnetic saturation is achieved at $B_s \approx 5$ and 13.5 T for A = Rb and K, respectively (see also Ref. [33]).

C. Specific-heat data

Finally, we analyze the specific-heat data of the three compounds that have been measured in the temperature range between 2 and 300 K in zero and magnetic fields up to 8 T. Isotypic nonmagnetic compounds have been used to account for the lattice contribution to the respective total specific heat. The left panels of Fig. 5 show the magnetic part of the specific heat for $A\mathrm{Ag}_2\mathrm{Cr}[\mathrm{VO}_4]_2$, with A = Ag, K, and Rb. The distorted TL (A = Ag) exhibits a λ anomaly at $T_N \approx 10$ K, which is not affected by high magnetic fields. We estimate the interlayer coupling constant ($J_{\mathrm{inter}}^{\mathrm{Ag}} \approx 0.1$ K) from fitting $C_m \propto T^3$ [36] consistent with our density-functional theory (DFT) calculations (see below).
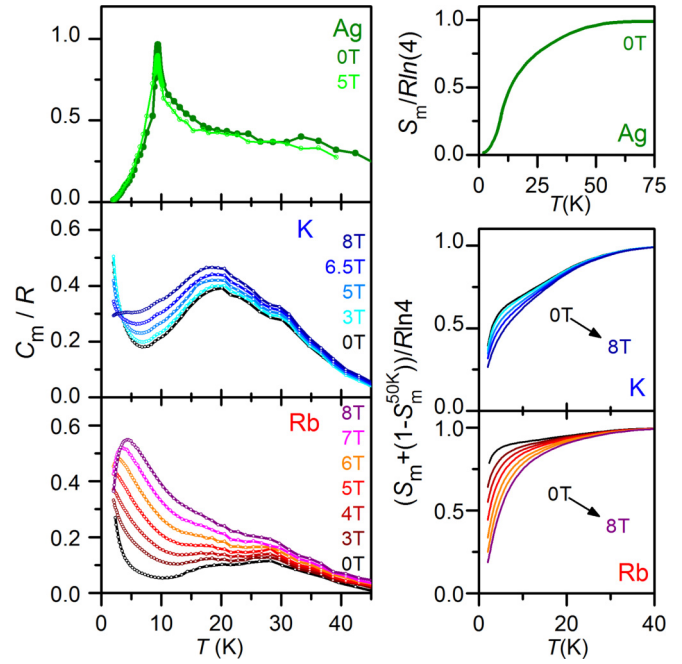
In contrast to the Ag compound, the undistorted TL cases (A = K and Rb; space group $P\bar{3}$) show significantly different behavior in $C_m(T)$ and reveal drastic field dependencies. In particular, the Rb compound develops a broad maximum in $C_m(T)$ which shifts to higher temperatures with increasing magnetic fields, suggesting the opening of a field-induced gap in the magnetic excitation spectrum. Interestingly, the data suggest the existence of a crossing point of the various $C_m(T, B = \mathrm{const})$ around 1 K, unfortunately out of the accessible temperature range of our experiment. For the K compound, however, such a crossing point is revealed around 3 K. According to Ref. [37], such an isosbestic point is accompanied by extremal values of $d\chi(T)/dT$ at slightly lower temperatures and discussed as thermodynamic signatures of the crossover from a high-temperature paramagnetic phase to a low-temperature SL phase. In fact, we observe such extrema in $d\chi(T)/dT$ around 3 K for the A = K compound and around 0.6 K for A = Rb (see Ref. [33]), suggestive of the crossover into a low-temperature SL phase.

The derived spin entropy data for the series are shown in the right panels of Fig. 5. For the Ag compound the maximum value of $R\ln 4 = S_m^{\max}$ is reached above $T \approx 50$ K. For the K and Rb compounds we shifted the individual curves representing the released spin entropy due to magnetic correlations above 2 K to their values at 50 K. It is noteworthy that for A = Rb (K) almost 80% (50%) of the total spin entropy is retained below $T = 2$ K in zero field, which supports a SL ground state. At high magnetic fields the spin entropy release above 2 K increases significantly for A = Rb and approaches $\approx 75\%$ of $S_m^{\max}$ at 8 T. The K compound behaves similarly but overall is less sensitive to magnetic fields.

D. *Ab initio* calculations

As pointed out above, we find differences in the dominant nearest-neighbor (NN) exchange for this series of Cr compounds. In our experimental work we have demonstrated a significant suppression of LRO from 10 K ($A =$ Ag) to at least 0.031 K ($A =$ K, Rb) by reducing the structural distortion of the TL and the [CrO$_6$] complex. The undistorted TL ($P\bar{3}$) allows only for small differences in angles for the local symmetry of the [CrO$_6$] complex (D_{3d} and O_h). The calculated single-ion anisotropies for Cr^{3+} in the AAg$_2$Cr[VO$_4$]$_2$ series reveal a c anisotropy for the magnetic moment with $M_\parallel^a \approx 0.46$ K and $M_\parallel^b \approx 0.88$ K for $A =$ Ag and $M_\parallel^a = M_\parallel^b \approx 0.66$ K for $A =$ K and Rb, above the lowest-energy state. These estimated values are very small indeed and similar to those reported for ACrO$_2$, which is considered an easy-axis Heisenberg TL [21]. At any rate, the reduction of the experimental J couplings from 3 K (Ag) to 0.5 K (Rb) cannot be explained purely on the basis of single-ion anisotropies.

In order to understand these experimental findings we performed electronic structure calculations with DFT methods and extracted the magnetic exchange constants by mapping total DFT energy differences of various spin configurations onto the Heisenberg Hamiltonian [38–40]. For further results and technical details see Refs. [33,41,42]. Analysis of the electronic band structure shows a considerable overlap of V-O states with empty Cr orbitals ($d_{z^2 - r^2}$ and $d_{x^2 - y^2}$) for $A =$ K, Rb which effectively reduce the ligand field splitting of the [CrO$_6$] complex with respect to $A =$ Ag. For calculating the exchange couplings we performed local-density approximation $+ U$ calculations and chose values of U that provide J values compatible with the experimental Θ_{CW} values.

The evaluation of the intraplane exchange couplings confirms an anisotropic TL model for $A =$ Ag with $J_1^{Ag} \approx 2/3 J_2^{Ag}$ representing the Cr-Cr distances along [010] assigned to J_1^{Ag} and the almost equal [110] and [$-$110] directions assigned to J_2^{Ag}. The small difference for the calculated $J_{2a}^{Ag} = 4.69(1)$ K for [$-$110] and $J_{2b}^{Ag} = 4.74(1)$ K for [110] is remarkable, as these coupling constants are apparently decisive for the magnetically ordered structure as determined by neutron powder diffraction data (see above). Note that these findings are compatible with a columnar AFM, in line with theoretical work on the anisotropic triangular Heisenberg AFM lattice and the topologically equivalent square lattice with one diagonal bond (see, for reference, [43]).

For the isotropic TL we calculate $J_1^K = 2.8$ K, which is similar to J_1^{Ag}, and a significantly reduced $J_1^{Rb} = 0.4$ K. These (NN) values are in reasonable agreement with the values extracted from the susceptibility measurements. Additionally,

DFT calculations allow us to disentangle contributions coming from further exchange paths. Overall, intraplane second (NN) exchange couplings are rather small ($\approx$0.01 K) throughout the series and not significant to explain the suppression of LRO to such an extent.

We address now the differences in the interplanar exchange couplings. These follow two principal stacking types with different relative orientations of the TL along the stacking direction: (i) alternating ABA and (ii) identical AA stacking sequences. First, we comment on the Ag compound representing the ABA case ($C2/c$). Here, we obtain a weak FM coupling constant, $J_3^{Ag} = -0.06$ K, or 2% in terms of J_1^{Ag}, in nice agreement with our magnetic structure from NPD. In contrast, the interlayer coupling for the AA stacking ($P\bar{3}$) is different in two aspects. First, these exchange couplings are AFM. Second, the interlayer coupling constants are about 10% of their respective $J_1^{K,Rb}$ values. Despite the significant amount of the interlayer exchange couplings, the undistorted TL reveal no signs of LRO, as shown in the experiments above.

IV. CONCLUSIONS

In conclusion, we showed the drastic reduction of LRO on the AFM TL from 10 K to temperatures at least lower than 0.031 K for a series of $S = 3/2$ compounds, AAg$_2$Cr[VO$_4$]$_2$, by altering the size of nonmagnetic spacers ($A =$ Ag, K, Rb) between magnetic layers. Our experimental data are consistent with a low-temperature SL phase for the undistorted TL ($A =$ K and Rb). We noted an effective reduction of J_1^{Rb} compared with J_1^K, despite the same Cr-Cr distances and only minor variations in Cr-O-Cr angles of less than $\pm 2°$. Structurally, this relates to the differences in the relative orientation of the [VO$_4$] linkers (coplanar with the TL) while the high symmetry (threefold rotation axis) is retained. Electronically, the enhanced hybridization Cr $3d$-O $2p$-V $3d$-O $2p$-Cr $3d$ and the isotropic exchange within the AFM TL are pronounced features of these SL candidates. Further explorations into additional higher-order exchange for complex linkers on the undistorted TL are called for and are beyond the focus of this experimental work.

[1] X.-G. Wen, Phys. Rev. B **65**, 165113 (2002).

[2] L. Balents, Nature (London) **464**, 199 (2010).

[3] F. Mila, Eur. J. Phys. **21**, 499 (2000).

[4] C. Wang and T. Senthil, Phys. Rev. B **91**, 195109 (2015).

[5] L. Savary and L. Balents, Rep. Prog. Phys. **80**, 016502 (2017), see Table 1 and Chaps. 6.1 and 6.44.

[6] T.-H. Han, J. S. Helton, S. Chu, D. G. Nocera, J. A. Rodriguez-Rivera, C. Broholm, and Y. S. Lee, Nature (London) **492**, 406 (2012).

[7] B. J. Powell and R. H. McKenzie, Rep. Prog. Phys. **74**, 056501 (2011).

[8] T. Isono, T. Terashima, K. Miyagawa, K. Kanoda, and S. Uji, Nat. Commun. **7**, 13494 (2016).

[9] A. P. Ramirez, Annu. Rev. Mater. Sci. **24**, 453 (1994).

[10] A. Yu. Kitaev, Ann. Phys. (N.Y.) **303**, 2 (2003).

[11] J. Chaloupka, G. Jackeli, and G. Khaliullin, Phys. Rev. Lett. **105**, 027204 (2010).

[12] Y. Shirata, H. Tanaka, A. Matsuo, and K. Kindo, Phys. Rev. Lett. **108**, 057205 (2012).

[13] J. Ma, Y. Kamiya, T. Hong, H. B. Cao, G. Ehlers, W. Tian, C. D. Batista, Z. L. Dun, H. D. Zhou, and M. Matsuda, Phys. Rev. Lett. **116**, 087201 (2016).

[14] B. Bernu, C. Lhuillier, and L. Pierre, Phys. Rev. Lett. **69**, 2590 (1992).

[15] H. Kawamura, J. Phys. Condens. Matter **10**, 4707 (1998).

[16] L. Capriotti, A. E. Trumper, and S. Sorella, Phys. Rev. Lett. **82**, 3899 (1999).

[17] G. H. Wannier, Phys. Rev. **79**, 357 (1950).

[18] S. Seki, Y. Onose, and Y. Tokura, Phys. Rev. Lett. **101**, 067204 (2008).

[19] M. Kenzelmann, G. Lawes, A. B. Harris, G. Gasparovic, C. Broholm, A. P. Ramirez, G. A. Jorge, M. Jaime, S. Park, Q. Huang, A. Ya. Shapiro, and L. A. Demianets, Phys. Rev. Lett. **98**, 267205 (2007).

[20] N. E. Amuneke, J. Tapp, C. R. de la Cruz, and A. Möller, Chem. Mater. **26**, 5930 (2014).

[21] A. Olariu, P. Mendels, F. Bert, B. G. Ueland, P. Schiffer, R. F. Berger, and R. J. Cava, Phys. Rev. Lett. **97**, 167203 (2006).

[22] E. Ghorbani, L. F. Tocchio, and F. Becca, Phys. Rev. B **93**, 085111 (2016).

[23] Y. Iqbal, W.-J. Hu, R. Thomale, D. Poilblanc, and F. Becca, Phys. Rev. B **93**, 144411 (2016).

[24] G. Misguich, C. Lhuillier, B. Bernu, and C. Waldtmann, Phys. Rev. B **60**, 1064 (1999).

[25] W. LiMing, G. Misguich, P. Sindzingre, and C. Lhuillier, Phys. Rev. B **62**, 6372 (2000).

[26] M. Holt, B. J. Powell, and J. Merino, Phys. Rev. B **89**, 174415 (2014).

[27] M. Roger, J. H. Hetherington, and J. M. Delrieu, Rev. Mod. Phys. **55**, 1 (1983).

[28] *Magnetic Interactions in Molecules and Solids*, edited by C. de Graaf and R. Broer (Springer, Cham, 2016), Chap. 5.42.

[29] A. Möller, N. E. Amuneke, P. Daniel, B. Lorenz, C. R. de la Cruz, M. Gooch, and P. C. W. Chu, Phys. Rev. B **85**, 214422 (2012).

[30] A. A. Tsirlin, A. Möller, B. Lorenz, Y. Skourski, and H. Rosner, Phys. Rev. B **85**, 014401 (2012).

[31] J. Rodríguez-Carvajal, Physica B **192**, 55 (1993).

[32] G. A. Bain and J. F. Berry, J. Chem. Educ. **85**, 532 (2008).

[33] See Supplemental Material at http://link.aps.org/supplemental/10.1103/PhysRevB.96.064404 for additional experimental and theoretical details, which includes Refs. [37–42].

[34] M. Gerloch and R. F. McMeeking, J. Chem. Soc. Dalton Trans. 2443 (1975).

[35] C. Delmas, G. Le Flem, C. Fouassier, and P. Hagenmuller, J. Phys. Chem. Solids **39**, 55 (1978).

[36] A. Du, G. Z. Wei, and J. Li, Phys. Status Solidi B **234**, 636 (2002).

[37] A. P. Ramirez, B. Hessen, and M. Winklemann, Phys. Rev. Lett. **84**, 2957 (2000).

[38] K. Koepernik and H. Eschrig, Phys. Rev. B **59**, 1743 (1999); FPLO, http://www.FPLO.de.

[39] J. P. Perdew, K. Burke, and M. Ernzerhof, Phys. Rev. Lett. **77**, 3865 (1996).

[40] A. I. Liechtenstein, V. I. Anisimov, and J. Zaanen, Phys. Rev. B **52**, R5467(R) (1995).

[41] T. Mizokawa and A. Fujimori, Phys. Rev. B **54**, 5368 (1996).

[42] H. O. Jeschke, F. Salvat-Pujol, and R. Valentí, Phys. Rev. B **88**, 075106 (2013).

[43] B. Schmidt and P. Thalmeier, Phys. Rev. B **89**, 184402 (2014).